Thermal integration of a high-temperature co-electrolyzer and experimental methanator for Power-to-Gas energy storage system

Thermal integration of a high-temperature co-electrolyzer and experimental methanator for Power-to-Gas energy storage system

M. A. Ancona[a], V.Antonucci[b], L. Branchini[a], F. Catena[a], A. De Pascale[a*], A. Di Blasi[b], M. Ferraro[b], C. Italiano[b], F. Melino[a], A. Vita[b]

[a] Alma Mater Studiorum, Università di Bologna - DIN, viale del Risorgimento 2, Bologna, 40136, Italy

[b] CNR-ITAE, Salita S. Lucia sopra Contesse 5, Messina, 98126, Italy

*****corresponding author:

Abstract

Performance of an innovative storage system for renewable energy, based on the Power-to-Gas concept are numerically predicted. The investigated system is composed by a high temperature co-electrolyzer of Solid Oxide Electrolyte Cell technology and an experimental methanation section, based on structured catalyst, suitable for high temperature operation. With the aim to thermally integrate high temperature co-electrolysis and methanation, a parametric thermodynamic analysis of the Power-to-Gas system is carried-out with a lumped-parameters approach, including all the thermal and electric energy consumptions. In particular, in order to optimize the system thermal balance of plant, various configurations involving internal heat recovery and pressurization of components are also considered. Numerical results are provided in terms of different performance indicators, such as electric-to-fuel conversion index, first law efficiency and second law efficiency and output-fuel quality indicators. The study demonstrates the possibility to thermally integrate the co-electrolyzer and the high-temperature methanation section achieving significant energy savings. Moreover, the calculated results show that the system set-up providing higher quality of the produced synthetic natural gas do not always lead to larger values in energy conversion efficiency. Eventually, advanced configurations of the Power-to-Gas system including heat recovery allow to achieve first-law efficiency up to values around 80-85% and second-law efficiency around 70-78%; a second methanation section based on conventional low-temperature reactors is included in the system and pressurization of the methanation section, or pressurization of the co-electrolysis section, is mandatory, in order to achieve large fraction of methane (up to 95-99%) in the produced synthetic fuel.

* Corresponding author

Keywords: Power-to-Gas; storage system; co-electrolysis; methanation; SNG; parametric analysis.

1. Introduction

In recent years, great emphasis has been given to renewable energy sources by the energy policies in many countries and enormous efforts have been put to replace conventional sources, with the aim to reduce greenhouse gases (GHGs) emissions. Also due to the public and private assets invested in research and development, these "green" power generation technologies have undergone a high penetration rate in the energy market, covering around 23% of the world total production of electric energy and about 30% in Europe, in 2017 [1]. However, these resources have their own drawback. Indeed, the incoming of so-called Non-Programmable Renewable Energy Sources (NP-RES) in the electric system has involved new risks and it has made worse existing problems in the management of local and regional electric networks, as reviewed in [2]. Among critical issues induced by the introduction of NP-RES, the deterioration of electric services and the fluctuating and intermittent power production by NP-RES, like wind and solar, are the most important. In particular, Eltawil et al. [3] have evaluated the operation of grid-connected photovoltaic (PV) generators, demonstrating that control problems can be registered as a consequence of the variable power generation. Furthermore, significant variations in power flows on transmission lines can occur, due to changes in climate conditions, and they may lead to the need of modifications in system protections and power control practices [4]. Therefore, long term and large capacity electricity storage devices are required. Several proposed energy storage technologies (state-of-the-art reviews can be found for example in [5]) can be categorized in: (*i*) electrical, (*ii*) mechanical, (*iii*) electrochemical, and (*iv*) chemical. The application of different typologies of storage devices in electrical grids has been deeply investigated: as an example, a comparison of flywheels utilization with respect to batteries for micro-grids has been analyzed in [6], while a comprehensive review of the characteristics of several systems is given in [7], with a discussion on their technological development status and capital costs. Finally, real life applications of storage devices are investigated in [8], highlighting the future challenges and prospects of the sector, while the regulatory aspects and market design challenges of grid-integrated storage are discussed in [9].

Among all the storage solutions suggested as ancillary to the renewable sources, the Power-to-Gas (P2G) chemical storage concept offers an interesting prospect [10], primarily in terms of available capacity. A P2G system basically allows to obtain storable synthetic fuels (*i.e.*, hydrogen, methane, synthetic natural gas, etc.), using the surplus of electric power produced from NP-RES (mainly photovoltaic and wind generators) [11]. To this respect, economic evaluations have been carried out in [12], considering the process chains of different power-to-gas paths (including their suitability for applications and the optional methanation step, as well as distribution options and end-user applications).

In detail, the full P2G process for synthetic natural gas (SNG) generation essentially consists in hydrogen production (H_2), through water (H_2O) electrolysis, and the successive hydrogen catalytic conversion into a methane (CH_4) rich fuel, by a methanation section. In [13], an interesting review of the last century research on methanation is given, focusing both on reaction mechanisms and technology development and modelling. Furthermore, relating to the methanation process, it should be considered that it requires also carbon dioxide (CO_2) as reactant: this capability to recycle CO_2 is another relevant advantage of a P2G storage system, towards the mitigation of the climate change issue involved by the power generation and other sectors. Indeed, the amount of CO_2 required by the P2G system can be provided by power plants run on conventional fuels, by other carbon intensive industrial sectors (*e.g.*,. cement and ammonia production processes) or by biomass conversion processes [14]. Therefore, a P2G technology coupled with carbon capture and storage (CCS) systems [15] can be also considered a potential pathway for decarbonisation of power and industrial sectors. A very recent review of projected P2G deployment scenarios proposed to date at regional and distributed scales is presented by Eveloy et al. in [16].

One of the key components requiring proper design for the P2G application is the electrolyzer. To this respect, Buttler et al. [17] present a literature review, based on an extensive market survey, on the current status of water electrolysis for energy storage, highlighting the different levels of technological development between low and high temperature electrolyzers. Indeed, low temperature water electrolyzers (LTE), operating below 100 °C and based on PEM (Proton Exchange Membrane) or Potassium Hydroxide (KOH) electrolyte technologies, are currently commercial products [18]. High-temperature steam electrolyzers (HTE), typically operating in the range 600-1000 °C and based on the Solid Oxide Electrolysis Cell (SOEC) technology [19], instead, are still at the pre-commercial stage for multi-kW-range size (*e.g.*, see the HELMETH EU project [20]). Nevertheless, HTE expected efficiency is very promising: values nearly 100% (if thermal integration is considered) are mentioned in a very recent review paper [21], remarkably higher in comparison with the current LTE efficiency level (average values can be estimated around 50-70%) [22]. The P2G whole system efficiency based on HTE has been targeted to values around 70-75% on HHV basis [23]. To demonstrate the advantages of HTE, few lab-scale or pilot plants have been built in recent years, even if the large part of pilot and demonstration plant still use LTE, as summarized in [24].

In this context, the research novelty of this study mainly stands in the development and analysis of an innovative and efficient P2G system, considering the possibility to thermally integrate the electrolysis with the methanation process, as a first step towards a physical integration between the two components. As a consequence, for the higher expected efficiency and temperature levels (since methanation typically requires operating temperatures between 200-700 °C [12]), in this study HTE has been considered for the P2G application. In particular, high temperature SOEC technology co-electrolysis – *i.e.*, simultaneous production of H_2 and carbon monoxide (CO) by co-feeding the electrolyzer with H_2O and CO_2 – is taken into account and included in the P2G storage system under investigation. Indeed, co-electrolysis allows (*i*) to achieve conversion

efficiency values more than five percentage points higher than the steam electrolysis case, as already calculated in a study by Giglio et al. [25], and (*ii*) to directly couple the SOEC with the inlet stream of CO_2, simplifying the subsequent methanation reactor feeding system design.

In addition, another important feature of the investigated P2G system, which leads to the innovative arrangement proposed in this study, is the coupling of the co-electrolyzer with a downstream experimental methanation reactor. This advanced methanation reactor consists in a fixed-bed reactor with a new formulation of structured catalyst, which allows to operate at relatively high temperatures, as already demonstrated in laboratory scale experiments by Vita et al. [26]. The proposed P2G system is finally composed by a SNG conditioning section, in order to reach the SNG quality for the introduction into the natural gas network.

With respect to Authors' previous studies – in which preliminary analysis on high temperature electrolysis [27] and on performance improvement, achievable with the co-electrolysis [28], have been carried out – the aim of this paper, as previously mentioned, is to develop an innovative integrated P2G system, conceiving the SOEC co-electrolyzer and the experimental reactor as a thermally integrated system and assessing their optimum internal thermal design conditions. The thermal synergy can be achieved operating both the co-electrolyzer and the methanation sections within relatively high temperature ranges (in particular, the co-electrolysis operation at intermediate temperature has been recently demonstrated in a work by Lo Faro et al. [29]). In order to demonstrate the feasibility of similar operating temperature levels (for both the co-electrolyzer and the experimental methanation reactor) and to achieve significant energy savings by means of proper internal heat recovery, several configurations of the proposed P2G system are presented, investigated and compared in terms of energy storage performance, via a thermo-chemical numerical study of the process.

In particular, in section 2 of the paper the P2G system is described in a basic layout arrangement, not including heat recovery (Reference Case); the system components are described and a numerical thermodynamic model of the P2G is implemented. In section 3, the variants of the P2G system with heat recovery, taken into account to improve the thermal integration between components, are illustrated. In section 4 the main performance parameters used in the paper to compare the different variants are introduced. Finally, the obtained results are provided and discussed in section 5.

2. The Power-to-Gas system: description and model

A simplified block diagram of the innovative P2G system analyzed in this work is shown in **Fig.1**, where the key components and the main flows are highlighted. The storage system receives, as main input materials, both water and carbon dioxide, provided by external sources, and it delivers high quality SNG, as main output, to the natural gas (NG) network.

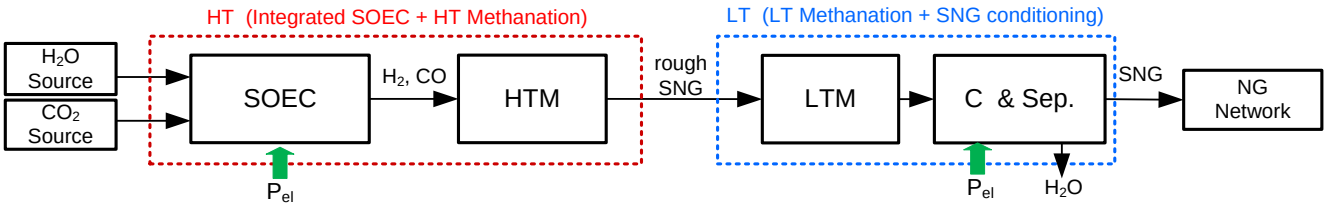

Fig. 1. Simplified block diagram of the P2G system.

The system is composed by an upstream high-temperature (HT) SNG production section (highlighted in red in **Fig.1**) and a downstream low-temperature (LT) SNG conditioning section (in blue in figure).

The HT section is the key section of the P2G system and it comprises the following main components:

- a co-electrolyzer (SOEC in figure), where co-electrolysis reactions of H_2O and CO_2 occur, by means of the main electric power input to the P2G storage system; the SOEC produces the converted species, including hydrogen and carbon oxide as main output;
- a high temperature methanation (HTM) sub-section, based on the National Research Council (CNR)-tested experimental reactor [26], producing a rough SNG stream (containing CH_4 and other components) to be conditioned.

This HT section represents the core and innovative device of the proposed P2G system. The subsequent LT section is implemented, in order to improve quality of the rough SNG from the upstream HT section. In particular, the LT section is composed by:

- a low temperature methanation (LTM) sub-section, based on conventional catalytic methanation technology (TREMP™ [30]); this additional methanation section has been included in the study in order to increase the CH_4 content of SNG prior to its storage;
- a further SNG processing section, where the SNG is mainly compressed, cooled and separated from residual water, before the introduction into the NG distribution network.

The involved thermal flows and the required heat exchangers are not shown in **Fig. 1** for sake of simplicity, as they will be identified in detail in the following paragraphs. Regarding the operating temperature and pressure levels and the heat recovery arrangement, all of these design settings have been the subject of an in-depth comparative analysis among several configurations.

In the following section, the basic configuration (named Reference Case) of the P2G system is presented; the developed lumped parameter model for the entire P2G system, comprising sub-models of the SOEC, of the methanation sections and of the SNG compression and separation sections, is described in detail.

2.1 Reference Case

The basic thermal layout configuration of the P2G taken into account in this study, is shown in **Fig. 2**, where the reactors, the main power flows and heat exchangers are highlighted. The electric power input is considered entirely provided by RES generation.

The inlet streams of H_2O and CO_2 are preheated up to the SOEC operating temperature (typical temperature range equal to 600-950 °C [21, 31]) by means of external heaters.

The SOEC co-electrolyzer at the anode side is fed with preheated sweep air; the SOEC produces a stream of air rich of oxygen (O_2) at the anode outlet and CO and H_2 as main useful co-electrolysis reaction products at the cathode outlet.

The cathode outlet stream is cooled to the HTM operating temperature with the HX1 heat exchanger; based on the tests conditions [26] for the HTM reactor, the thermal operation range is 250-600°C. The HTM reactor produces a rough SNG, still hot and rich of unreacted components (CO_2, H_2O).

In order to improve the methane content in the rough SNG, the LTM sub-system, based on the TREMP™ [30] technology, the SNG compression and water separation are included in the SNG LT conditioning line. As the LTM, compression and separation sections present different and quite low optimal operating temperature levels, specific pre-coolers, inter-coolers and after-coolers are considered (HX2, HX3, HX4 heat exchangers in **Fig.2**). Additional cooling flows, not shown in detail in **Fig. 2**, will be involved in the LTM and SNG compression sections.

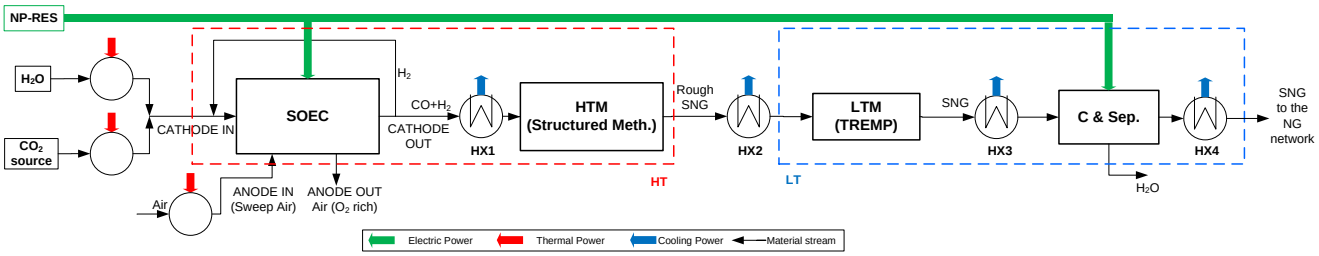

Fig. 2. Thermal layout of the P2G Reference Case.

This P2G system has been modeled on ASPEN Hysys™ environment [32], a commercial tool with lumped-parameters approach for numerical modeling of complex energy systems, able to perform steady-state thermo-chemical analysis of the process. Standard units from ASPEN Hysys™ library have been employed to model common components, like separators, heat exchangers, pumps and compressors; specific sub-models have been implemented for the key components of the P2G system.

Co-electrolyzer model

The first key component of the innovative P2G system is the high-temperature co-electrolyzer of SOEC technology. ASPEN Hysys™ does not contain a single prebuilt co-electrolyzer model. Therefore, in the developed SOEC model (**Fig. 3**) the co-electrolyzer has been designed as a combination of prebuilt units, according to [33], using three reactors (RI, R2 and R3 in **Fig. 3**) in order to simulate the main internal reactions.

In particular, co-electrolysis reactions (1), (2) of water and carbon dioxide occur in the conversion reactor R2:

$$H_2O \rightarrow H_2 + \frac{1}{2}O_2 \quad (1)$$

$$CO_2 \rightarrow CO + \frac{1}{2}O_2 \quad (2)$$

Moreover, the equilibrium reverse water-gas shift reaction (3) is considered by means of reactors R1 and R3:

$$CO_2 + H_2 \leftrightarrow CO + H_2O \quad (3)$$

In addition, for SOEC under pressurized conditions, methane formation may also take place [34, 35] through the following reaction (4):

$$CO + 3H_2 \leftrightarrow CH_4 + H_2O \quad (4)$$

Generally, in the modeling process it is considered that firstly the reactants reach the chemical equilibrium through the reverse water-gas shift reaction and then the co-electrolysis reactions occur. Finally, the produced syngas achieves the equilibrium according to (3) and (4) before leaving the cathode compartment [36-38].

The R3 outlet stream in **Fig. 3** corresponds to the outlet flows of the anodic compartment and of the cathodic compartment. The physical separation between the two sides of the electrolytic cell is modeled by a flow separator component (Sep1). The output stream from the anodic compartment is also modeled including the presence of the sweep air flow.

Preheated sweep air stream at the anode compartment is included in the model, in order to simulate the oxygen removal from the anode side of the SOEC stack and to account for the residual heat content. The sweep air stream has been set in order to achieve the 50% of oxygen molar fraction at the anode outlet stream [36].

A small percentage of hydrogen is recirculated from the cathode outlet to the inlet, to ensure reducing atmosphere and, thus, to avoid re-oxidation in the electrode [39]. The required amount of hydrogen, fixed in the model equal to 5% in volume of the inlet stream, is separated (via separator Sep2 and flow splitter Sep3 shown in **Fig. 3**, according to [27]) and then recirculated to the feed stream. It should be pointed out that the liquid outlet streams at each reactor are default settings of the software and calculated as zero in this sub-section.

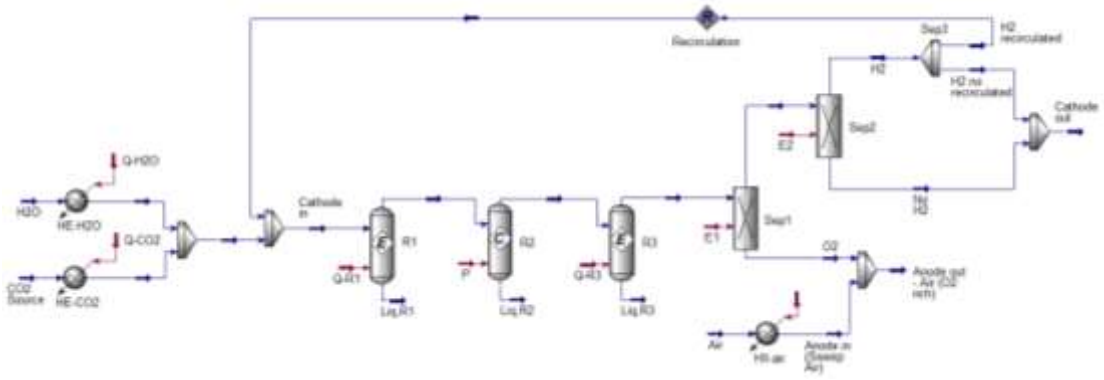

Fig. 3. SOEC sub-model developed on ASPEN Hysys™.

High Temperature Methanation section model

In the proposed P2G system, the SOEC cathode outlet syngas – rich in H_2, CO_2 and CO – is converted into a methane rich fuel, by means of the downstream high temperature methanation reactor (HTM in **Fig. 2**). This reactor is based on a structured catalyst developed and tested by CNR-ITAE at laboratory scale [26], considering its scaling at a large size.

The CNR-ITAE experimental reactor set-up consists in a quartz tubular fixed-bed reactor (horizontally placed in a furnace) under atmospheric pressure. The reactor contains a structured catalyst (diameter 1 cm, length 1.5 cm in the laboratory scale), with the catalytic layer (50 wt.% Nichel/Gadolinium-Doped-Ceria – Ni/GDC) deposited on the cordierite monolith (500 cps) by Solution Combustion Synthesis (SCS) reaching a total loading of 0.5 g/cm^3. Details on the catalyst features and on the experimental setup has been previously provided [26]. Briefly, the temperature dependence (250-600 °C) of the catalytic performance was evaluated with a supply of 11.1% CO_2/8.9% CO/68.9% H_2/11.1% N_2 at Gas Hourly Space Velocities (GHSV) of 10000, 30000 and 50000 h^{-1}. In these tests, the incoming molar fractions remain unchanged regardless of the flow analyzed. On the basis of the outlet flow composition, the reactor conversion rate (CR) has been calculated as:

$$CR = \frac{\dot{n}_{CH4,out}}{(\dot{n}_{CO}+\dot{n}_{CO2})_{in}} \quad (5)$$

where $\dot{n}_{CH4,out}$ represents the outlet molar flow of CH_4 and $(\dot{n}_{CO}+\dot{n}_{CO2})_{in}$ is the inlet molar flow of CO and CO_2. The trend of CR as a function of temperature and of the inlet flow has been analyzed (see **Fig. 4a**). It can be noted that, for the used structured catalyst, the production of methane is very low for temperatures below 300 °C and it increases with the operating temperature; the CR is maximum for temperature ranging around 400-500 °C, while it tends to reduce for temperature values above that interval, but it is still significant up to 600 °C. This upper range of values could be compatible with the SOEC operating conditions and, in particular, a good thermal matching between the two components can be found with an interposed heat exchanger (HX1 in **Fig. 2**), producing a limited gas cooling effect. It should be noted that during the carried-out tests, the experimental reactor temperature has shown a quite isothermal behavior along its length (**Fig. 4b**).

In order to simulate the HTM process on ASPEN Hysys™ environment, an isothermal conversion reactor has been used, setting CO and CO_2 conversion into CH_4 according to the Sabatier methanation reactions (6)-(7):

$$CO + 3H_2 \rightarrow CH_4 + H_2O \quad (6)$$

$$CO_2 + 4H_2 \rightarrow CH_4 + 2H_2O \quad (7)$$

The input values of CR have been modeled within ASPEN Hysys™ as a function of the operating temperature, by interpolation of the available experimental data with a second order polynomial equation:

$$CR = C_0 + C_1 T + C_2 T^2 \quad (8)$$

where T is the operating temperature of the reactor, while C_0, C_1 and C_2 are the tuned coefficients of the interpolating function. **Fig. 4a** shows the experimental data and the interpolating curve obtained for the 10000 GHSV case (red points in the figure), corresponding to the operative condition with maximum conversion rate, in the temperature range equal to 400-500 °C. The coefficients of the interpolating function plotted in **Fig. 4a** are: C_0 = -246.67; C_1 = 1.31; C_2 = $-1.37 \cdot 10^{-3}$.

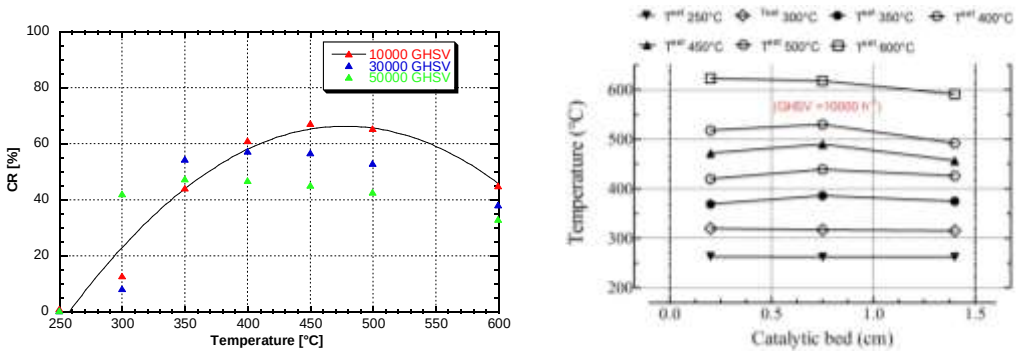

Fig. 4. a) Experimental Conversion Rate (CR) of the HTM, as a function of the operating temperature for three different values of inlet flow and interpolating function; b) Temperature profile of the catalytic bed.

Low Temperature Methanation section model

In order to simulate the LTM process, used to increase the methane content of the final output SNG, a methanation section with a multiple reactor arrangement, reproducing the Haldor-Topsøe TREMP™ [30] catalytic technology, is here considered. The TREMP™ technology is a well-known industrial process, usually operating in the temperature range of 250-700 °C, but the highest conversion efficiency values are typically achieved when operated close to the lowest values of the temperature range [40]; this process can be employed at large scale to produce synthetic natural gas, starting from several rough fuels varying from biomass to coal.

In this work, a multi-stage methanation section has been considered, using three equilibrium reactors (TREMP1, TREMP2 and TREMP3 in **Fig. 5**) located downstream the HTM experimental reactor (**Fig. 5**), in order to improve the overall system CH_4 production.

While the experimental reactor is modeled as isothermal, in order to match the experimental data [26], the TREMP™ reactors are modeled as adiabatic [30], *i.e.* the exothermic reactions will cause a temperature increase along the reactors from inlet to outlet. Thus, inter-cooling is included in the model between each reactor, in order to adjust the inlet temperature (LTM set temperature) for each equilibrium reactor. Also, in this sub-section the liquid outlet streams of each reactor are calculated as zero by the software.

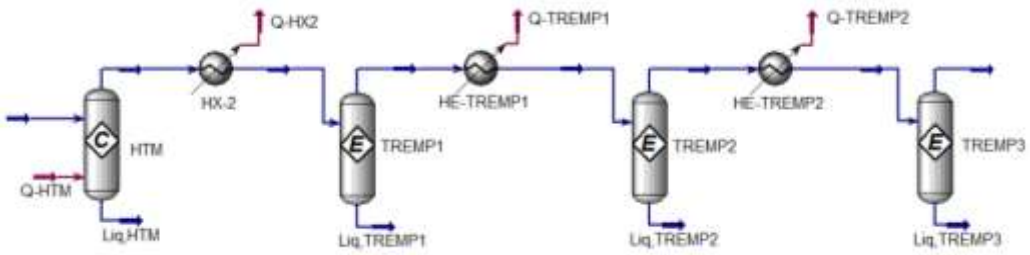

Fig. 5. HT and LT methanation sections model layout.

Synthetic natural gas compression and water separation

The methane-rich produced SNG is compressed and dehydrated with a gas treatment sub-system, depicted in **Fig. 6**. Power consumption of the compression line is included in the system electric demand. The SNG delivered by the upstream methanation sub-section is cooled to ambient conditions, to reduce the subsequent compression power absorption. The model comprises a two-step inter-cooled compressor, aftercooling and two water separators, which remove the residual liquid water, due to the gas cooling set-point temperature equal to 25 °C, for all the sub-section heat exchangers. The storage pressure has been set to 60 bar, corresponding to existing high-pressure NG pipelines. The compression isentropic efficiency has been set to 80%, in line with mean state-of-the-art NG compression station machines. Moreover, the compressor pressure ratio split has been optimized, in order to minimize the total compression work.

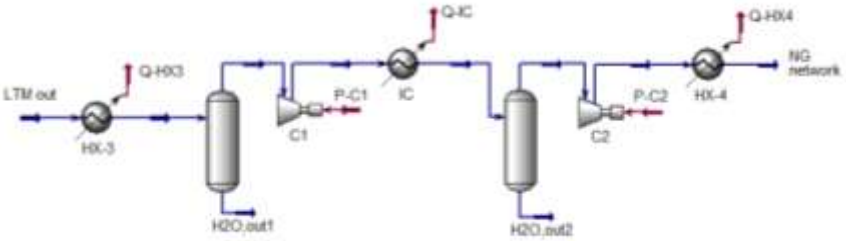

Fig. 6. Inter-cooled compression and water separation layout.

Reference Case power size and settings

The P2G system design power size considered in the study corresponds to a SOEC stack power size equal to 1MW of absorbed electric power. As a result, the thermodynamic analysis of the system and of all its variants has been carried out with a proper setting of the inlet H_2O and CO_2 mass flow rates, in order to keep the SOEC power size constant.

Moreover, in order to detect the optimum set-point conditions of the P2G feeding, a preliminary parametric analysis of the P2G system inlet stream composition has been carried out. The feeding composition in terms of H_2O/CO_2 split was changed, reducing stepwise the water fraction and increasing CO_2. In order to establish the optimal inlet stream composition, the stoichiometric conditions at the inlet of the HTM section (*i.e.* at the co-electrolyzer cathode outlet) have been targeted. The HTM FEED parameter calculated using the HTM inlet volume fractions, in stoichiometric conditions is defined as [25, 40]:

$$FEED = \frac{[H_2]-[CO_2]}{[CO]+[CO_2]} = 3 \quad (9)$$

The above reported FEED stoichiometric value leads to SNG with higher methane concentration, at the methanation outlet.

Results of the parametric assessment of inlet composition effects, presented in detail in a previous preliminary study on the system [28], show that only the P2G inlet composition with 80% H_2O and 20% CO_2 provide FEED values close to 3. Thus, this H_2O/CO_2 feeding ratio is used as set-point in this study.

The SOEC operating temperature in this Reference Case has been set equal to 850 °C, in line with high performance SOEC operating conditions, in accordance to the available literature on SOEC [41, 42]. Furthermore, experimental pilot plants [20] confirm the viability of the value set, in this study, for the SOEC operating temperature. In more detail, an experimental test – conducting for 700 hours of operation – has been carried out with the SOEC operating range between 845 and 855 °C, in order to evaluate the outlet stream composition. In addition, the conversion rate target of electrolysis reactions is assumed equal or higher than the 80 % in [20]: in this work, for a precautionary approach, a value equal to the 80 % is set.

On the other hand, the HTM operating temperature has been set equal to 450 °C, in order to exploit the HTM highest CR value, according to the experimental data in **Fig. 4a**.

The LTM (TREMP^{TM}) operating temperature has been set after a parametric study of its effect, considering – as already discussed – the typical temperature range of operation of this technology [30, 40]. The LTM operating temperature affects the outlet SNG composition, as shown in **Fig. 7**, presenting calculated values of the HTM outlet gas; the lower the operating temperature, the higher the methane concentration in the stream (methanation reactions are favored at low temperature). Thus, 200 °C has been selected as LTM temperature optimal set-point value.

Furthermore, the O_2 molar fraction within the anode outlet is set at 0.5, as suggested in [36].

Finally, the pressure at the outlet of the whole system has been assumed in order to allow the introduction of the produced SNG into the NG network, based on typical pressure values for high pressure ridges of Italian natural gas network [43].

Table 1 summarizes the Reference Case set point values of the P2G design parameters.

It should be highlighted that this Reference Case layout shows: (i) a remarkable high reactants preheating and (ii) several heat exchangers required to cool the main stream between the key sections, (the operating temperature is reduced from 850 °C at the SOEC, to 450 °C at the HTM and down to 200 °C at the LTM), but it does not include any internal heat recovery.

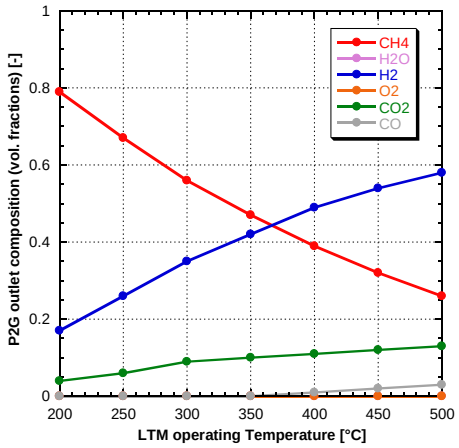

Fig 7. Reference Case outlet SNG composition, effect of LTM operating temperature.

Table 1. Main set point parameters of the P2G Reference Case.

Parameter	**Value**	**Units**
SOEC input electric power	1	MW
SOEC inlet H_2O fraction [20, 28]	80	%(vol.)
SOEC inlet CO_2 fraction [20, 28]	20	%(vol.)
SOEC operating temperature [20, 41, 42]	850	°C
H_2O electrolysis reaction Conversion Rate [20]	80	%
CO_2 electrolysis reaction Conversion Rate [20]	80	%
$x_{O2,anode\ out}$ [36]	0.5	-
HTM operating temperature	450	°C
LTM operating temperature [30, 40]	200	°C
NG distribution network pressure [43]	60	bar
P2G reactants feeding pressure	1	bar

3. Power-to-Gas system variants

In order to improve the internal balance-of-plant of the P2G system, the plant configuration can be rearranged, obtaining additional variants in terms of layout, operating temperature and pressure of components, and the thermal synergies among the sub-sections can be investigated. With this aim, the basic Reference Case configuration, presenting both the SOEC and the methanation sections operating at ambient pressure and without heat recovery within the system, has been the object of further layout optimizations. In more detail, additional variants of the P2G Reference Case have been considered, namely three layout cases including internal heat recovery (HR) and two cases with pressurized key components plus internal heat recovery (PHR). In particular, the following variant cases have been investigated:

- HR-1: internal heat recovery, same operating temperature and pressure values of the Reference Case;
- HR-2: internal heat recovery, reduced temperature for the SOEC section;

- HR-3: internal heat recovery, reduced temperature for the SOEC section and increased temperature for HTM;
- PHR-1: similar to HR-3, but with pressurized LTM;
- PHR-2: similar to HR-3, but with pressurized SOEC.

The HR-1, HR-2 and HR-3 Cases have been considered in order to quantify the benefits of heat recovery, in comparison with the Reference Case, and to analyze the effects of different operating temperature. The PHR-1 and PHR-2 Cases are proposed in order to investigate the additional effects of pressurizing the methanation and/or the SOEC components.

The detailed models (developed on ASPEN Hysys^{TM} environment) of the Reference Case and of the several variants are presented in Appendix A.

3.1 Reference Case with heat recovery

The layout of the variant case HR-1 is shown in **Fig. 8**. Internal heat recovery is introduced with the Heat Recovery Section (HRS in **Fig. 8**) to partially pre-heat the SOEC inlet H_2O stream, using heat available at different downstream sections of the P2G system. In more detail, heat is recovered from the SOEC outlet cathode and anode streams and from all the methanation reactors cooling sections. The pre-heating heat-exchangers arrangement in the heat recovery line has been established considering the temperature levels of the available heat flows. In particular, it has been decided to locate the pre-heating section in the more heat demanding H_2O line. Nevertheless, a residual external heat source is included to feed the SOEC with reactants at the internal operating temperature. The considered temperature set-point of the HR-1 Case for SOEC (850 °C) and for HTM (450 °C) and all the other operating parameters are the same of the Reference Case.

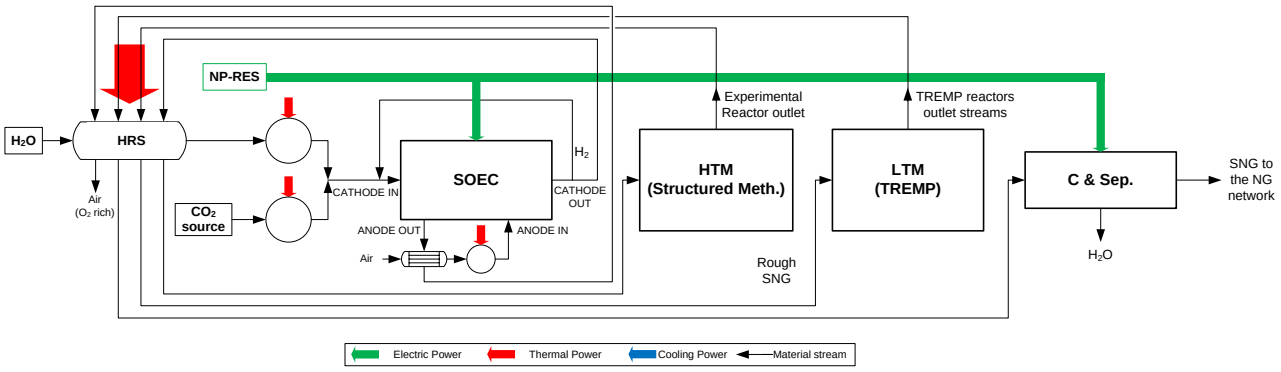

Fig. 8. Layout configuration of Case HR-1 and Case HR-2.

3.2 Heat recovery Cases with temperature variation

In order to test the effect of SOEC and HTM operating temperature, two additional cases, HR-2 and HR-3, have been considered and compared with case HR-1.

The Case HR-2 layout and heat recovery arrangement is similar to the HR-1 Case provided in **Fig. 8**, but it is characterized by a lower SOEC temperature value, equal to 600 °C. This reduction causes different SOEC electrochemical design, but in terms of thermal design it only leads to a reduced heat demand to preheat SOEC reactants and thus to different level of heat recovering in the pre-heating sections of Case HR-2, in comparison with Case HR-1.

In Case HR-3 the same temperature is considered for both the SOEC and the HTM reactor, equal to 600 °C. This change in HTM operating temperature leads to low but still acceptable performance (see **Fig. 4a**). This HR-3 configuration (shown in **Fig. 9**) does not require the heat exchange between the SOEC and HTM and thus allows to consider a direct SOEC-HTM thermally integrated arrangement. A temperature value of 600 °C of the two sub-systems can be considered as a good trade-off between the requirements of low operating temperatures for SOEC and high operating temperature values for HTM. The other operating parameters are kept in this Case the same of the Reference Case.

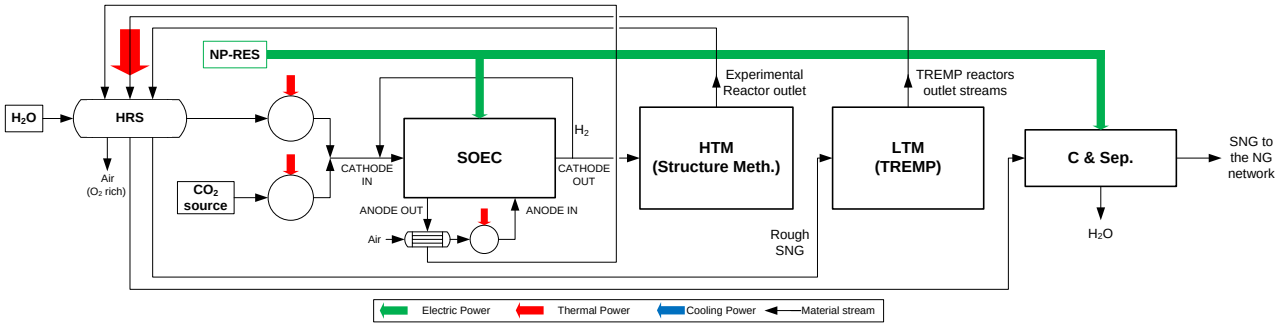

Fig. 9. Layout configuration of Case HR-3.

3.3 Heat recovery Cases with pressurized components

A further advancement has been considered by applying pressurization to the P2G system components of Case HR-3, in order to improve the methane content in the produced SNG (methanation reactions are favored at high pressure [44]).

In more detail, the first pressurized configuration Case PHR-1 (**Fig. 10a**) presents a pressurized LTM section obtained with the SNG processing section placed downstream of the experimental reactor. It must be highlighted that in this case, the outlet temperature of the SNG processing section is lower than the operating temperature of the LTM section and then a heater among the two sub-systems is required.

In **Fig. 10b** the configuration of Case PHR-2 is shown. In this case, the whole P2G system is pressurized with a pump (P) for the water inlet and with a gas compressor (C_{CO2}) at the CO_2 inlet steam. It must be noted that also the sweep air stream requires a compressor (C_{Air}), in order to reach the SOEC operating pressure. Moreover, in this case there is no need of the SNG compression section, since pressurization occurs at the inlet of the whole system, while residual water is still separated at the end of the process.

The operating temperature of the SOEC and HTM sections are considered equal to 600°C also in these cases and the pressurization level is set at the NG distribution network pressure.

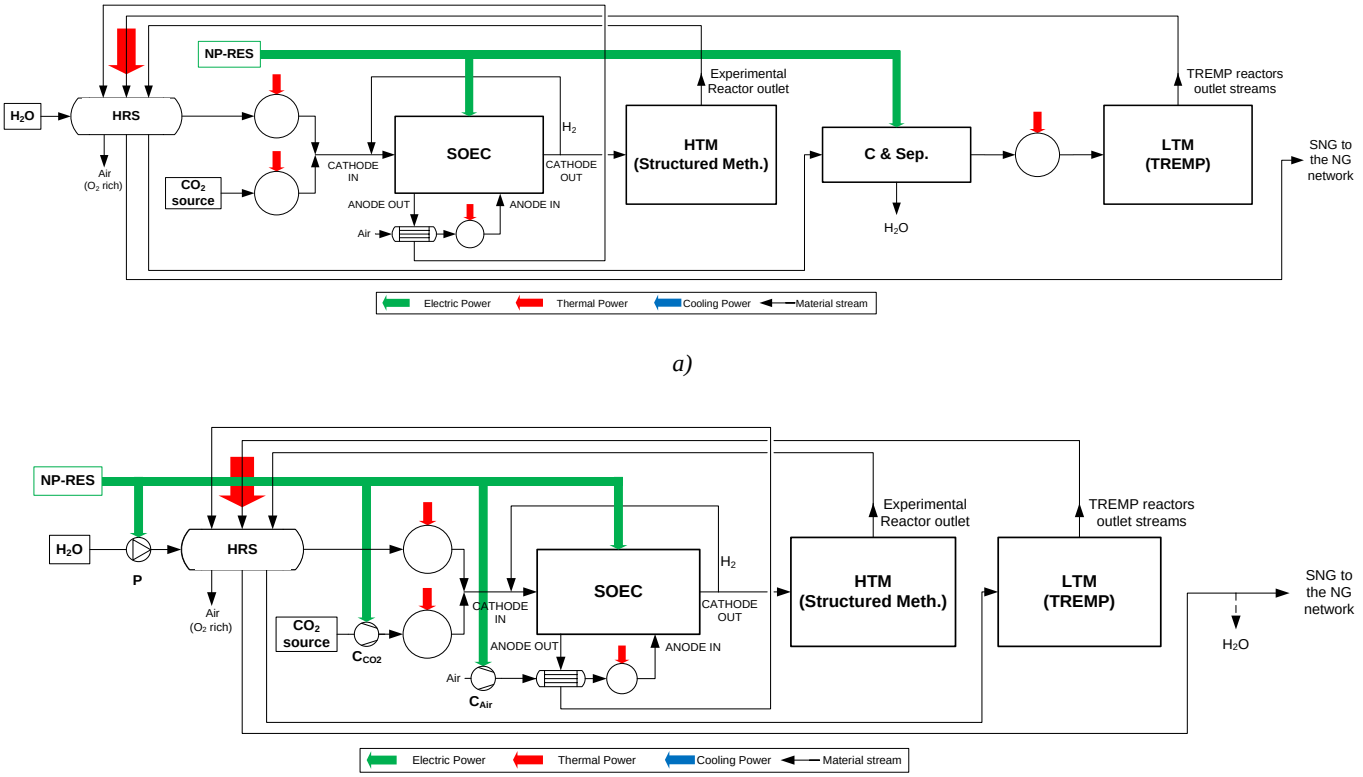

Fig. 10. Configuration of: a) Case PHR-1; b) Case PHR-2.

4. Performance parameters

Several performance parameters are considered and used in the analysis, in terms of energy conversion efficiency, thermodynamic efficiency (both via a first-law approach and with a second-law assessment) and quality parameters, taken into account in order to introduce the produced SNG into the natural gas distribution network.

In detail, the performance indicators applied for the P2G analysis are presented in the following list:

- The electric-to-fuel energy conversion index (referred to the higher heating content of the produced fuel), defined as follows:

$$\eta_{E2F} = \frac{\dot{m}_{SNG} \cdot HHV_{SNG}}{P_{e,IN}} \quad (10)$$

where $\dot{m}_{SNG}$ is the mass flow of produced SNG, HHV_{SNG} is the higher heating value of the SNG, $P_{e,IN}$ is the system inlet electric power, including both the co-SOEC input electric power and the auxiliaries electric power consumption.

- The first-law efficiency (referred to HHV), defined as follows:

$$\eta_I = \frac{\dot{m}_{SNG} \cdot HHV_{SNG}}{P_{e,IN} + Q_{IN}} \quad (11)$$

where Q_{IN} is the total amount of input heat required by the process.

- The second-law efficiency, defined as follows:

$$\eta_{II} = \frac{\dot{m}_{SNG} \cdot ex_{SNG}}{Ex_{in}} = \frac{\dot{m}_{SNG} \cdot ex_{SNG}}{Ex_{in,f} + Ex_{in,Q} + Ex_{in,Pe}} = \frac{\dot{m}_{SNG} \cdot ex_{SNG}}{\sum \dot{m}_{in} \cdot ex_{in,f} + Ex_{in,Q} + Ex_{in,Pe}} \quad (12)$$

where Ex_{in} represents the exergy of the system inlet mass streams, $Ex_{in,Q}$ the exergy of heat fluxes and $Ex_{in,Pe}$ the exergy related to the inlet electric power, while the corresponding mass specific exergy contributions are indicated as *ex*. Exergy represents the maximum useful work possible during a process that brings the system into equilibrium with surroundings environment [45, 46].

Mass specific exergy of inlet mass streams and outlet produced SNG are calculated as:

$$ex_{in,f} = ex_{in,Ph} + ex_{in,Mix} + ex_{in,Chem} \quad (13)$$

$$ex_{SNG} = ex_{SNG,Ph} + ex_{SNG,Mix} + ex_{SNG,Chem} \quad (14)$$

The above equations include the physical exergy ($ex_{in,Ph}$ and $ex_{SNG,Ph}$), a contribution related to components mixing ($ex_{in,Mix}$ and $ex_{SNG,Mix}$) and a chemical contribution ($ex_{in,Chem}$ and $ex_{SNG,Chem}$). The specific physical exergy is defined as:

$$ex_{Ph} = \Delta h - T_0 \Delta s = (h - h_0) - T_0(s - s_0) \quad (15)$$

where T_0, h_0 and s_0 are respectively temperature, specific enthalpy and specific entropy in reference conditions (T_0 = 25 °C, p_0 = 1 bar). Specific exergy of mixing type is defined as:

$$ex_{Mix} = \frac{R_0}{M_m} T_0 \sum_i \left[\ln\left(\frac{1}{y_i}\right) y_i \right] \quad (16)$$

where R_0 represents the universal gas constant, M_m the molecular mass of the mixture and y_i the molar fraction of the i-th component of the mixture.

Specific exergy of chemical type can be expressed as:

$$ex_{Chem} = \frac{1}{M_m} \sum_i \left(ex^0_{i,mol} \cdot y_i \right) \quad (17)$$

where $ex°_{i,mol}$ is the specific molar exergy related to a physical state of reference of the i-th component.

Finally, the exergy associated to a generic inlet heat term (Q) is defined as follows:

$$Ex_{in,Q} = Q\left(1 - \frac{T_0}{T}\right) \quad (18)$$

where T is the considered final heating temperature level at which Q is available.

- Quality of the output SNG. In order to consider that the produced SNG can contain various components besides methane, the following additional SNG quality parameters are monitored:
  - total output methane mass flow rate;
  - volume fraction of methane and residual species in the produced SNG;
  - LHV and HHV of the SNG;
  - specific gravity (SG) of the SNG, defined as the ratio between density of the produced gas and of the air;
  - Wobbe Index (WI), indicator of interchangeability of fuel gases with respect to natural gas, defined as:

$$WI = \frac{HHV}{\sqrt{\rho_{SNG}/\rho_{air}}} \quad (19)$$

where, ρ_{SNG} and ρ_{air} are respectively the density of the produced SNG and of the air [kg/Sm^3], both evaluated at *standard conditions* [47]. ρ_{air} has been set to a value equal to 1.22 kg/Sm^3.

5. Results and discussion

A comparative analysis among the several configurations is presented, highlighting the effect of the advanced variants with heat recovery, in comparison with the Reference Case configuration and demonstrating the viability of thermal integration between co-electrolysis and methanation.

The considered heat exchangers arrangement in the heat recovery line HRS and the temperature-heat diagram of each subsection are presented respectively in **Fig. 11** and **Fig. 12**, for all the examined configurations.

In case HR-1 (**Fig. 11a** and **Fig 12a**), the pre-heating section is composed by six heat exchanging segments (HE-1 to HE-6), recovering thermal power from the LTM section (three streams, *i.e.*, outlet of reactors TREMP1 TREMP2 and TREMP3), from the HTM section and from the SOEC (anode and cathode) outlet streams. The sequence of heat recovery segments along the line has been optimized in order to maximize the heat recovery effect.

It must be noted that in three heat exchangers (HE-3, HE-4 and HE-6) the exploitable hot side enthalpy is limited, since the hot stream outlet temperature is constrained by the downstream component; in the other three heat exchangers (HE-1, HE-2 and HE-5) the exploited temperature drop is given by the assumed minimum pinch between the hot and cold side, set equal to 5 °C.

With this arrangement, water starts to vaporize in the HE-2 section and, after the complete vaporization in HE-4, superheating

continues in the following two heat exchangers. At the outlet of the pre-heating section, steam is obtained with a temperature value of 842 °C.

Pre-heating section of case HR-2 (**Fig. 11b** and **Fig. 12b**) is similar to case HR-1, but different temperature levels occur, since the SOEC operating temperature is set at 600 °C. This reduced SOEC temperature affects the anode and cathode outlet streams, while temperature of the other recovered streams are nearly the same of the former case. As a consequence, the obtained steam outlet temperature is much lower than in case HR-1 (495 °C versus 842 °C).

Case HR-3 (**Fig. 11c** and **Fig. 12c**) presents a shorter HRS and a reduced pre-heating effect, since the SOEC and HTM operating temperature is the same and no heat recovery occurs between the two sub-systems. The increase in the HTM section operating temperature (600 °C) leads to a reduction of the HTM methanation performance and to a larger amount of reactants still in the outlet stream. As a consequence, the LTM section processes more reactants and the outlet temperature of each TREMP^{TM} reactor is higher. Even if the HRS number of segments is reduced, a steam is produced at relatively high temperature (590 °C), very close to the SOEC operating condition.

Also in case PHR-1 (**Fig. 11d** and **Fig. 12d**) the pre-heating section is composed by five segments, producing a remarkable pre-heating effect, but lower than in the HR-3 case (HRS outlet temperature equal to 507 °C). In this pressurized case the LTM reactors (and the downstream HRS segments) are more stressed, due to the larger amount of reactants to be processed and increased methanation effects; the calculated TREMP2 outlet temperature is 600 °C and the TREMP1 outlet temperature is over 800 °C; this is due to the simplified adopted settings of the reactors, modeled as adiabatic equilibrium reactors. These temperature values (close or outside the conventional operating range of this commercial technology, *i.e.*, 250-700 °C) represent an issue for the materials, to be more deeply analyzed in further studies.

Finally, for case PHR-2 (**Fig. 11e** and **Fig 12e**), even if the operating temperatures of the P2G key sections are the same of the previous case, a different HRS arrangement is obtained, composed by six segments. In this case, the pressurized water evaporation occurs at a higher temperature (277 °C). Moreover, the sweep air is compressed and thus heated by the compressor C_{Air}. Then, less thermal power is recovered in the pre-heating air line, obtaining a temperature value at the anode outlet (equal to 425 °C) higher than in the PHR-1 case; this enthalpy content can be exploited using two segments placed in different positions on the feed water line in order to optimize the heat recovery, on the basis of the temperature levels. Nevertheless, the resulting arrangement allows to recover less heat than in the previous case.

The values of thermal power exchanged at each segment of the HRS are provided in **Table 2**, along with the external heat demand.

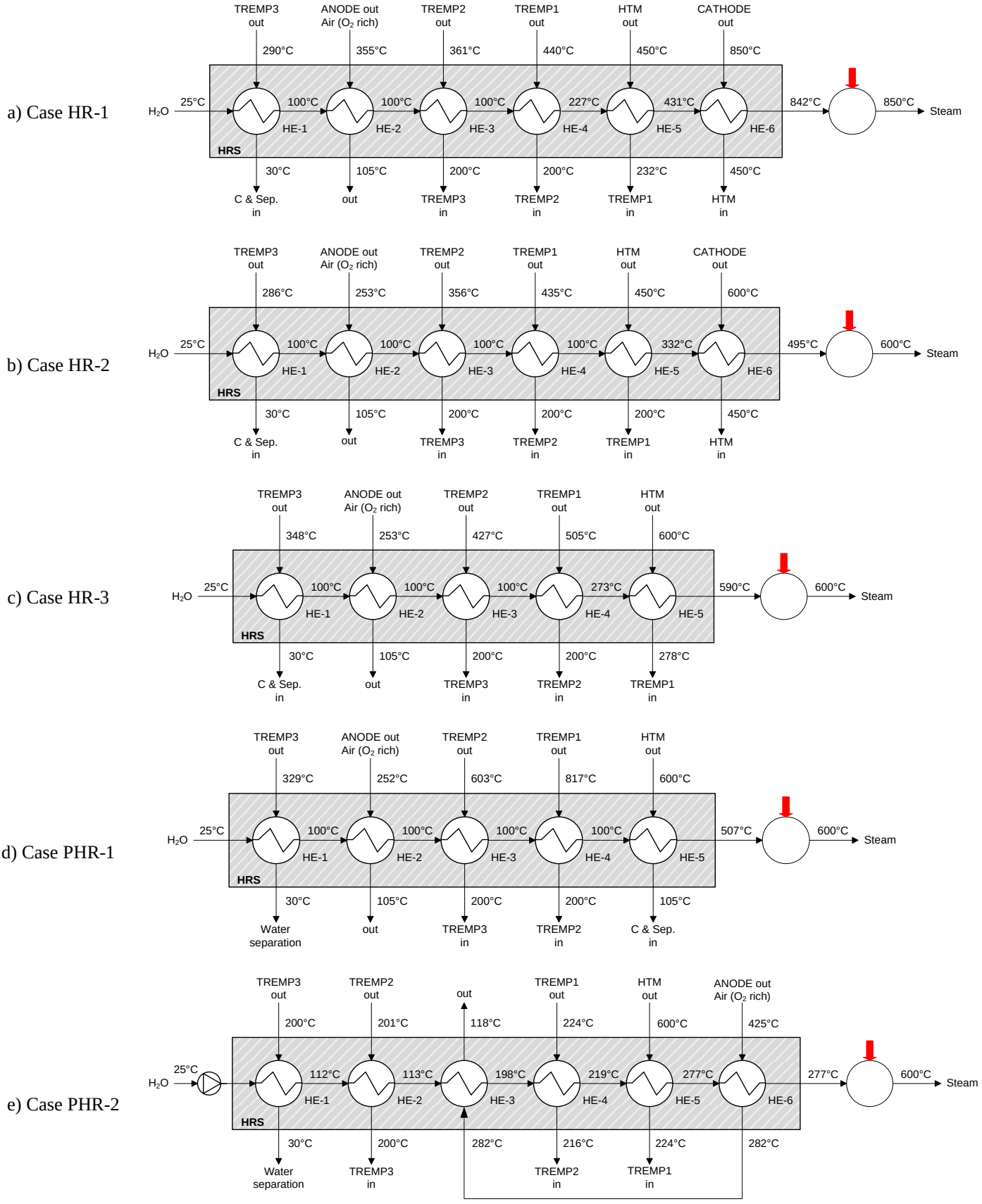

460 **Fig. 11.** Thermodynamic design of the heat recovery section HRS: a) case HR-1; b) case HR-2; c) case HR-3; d) case PHR-1; e) case PHR-2.

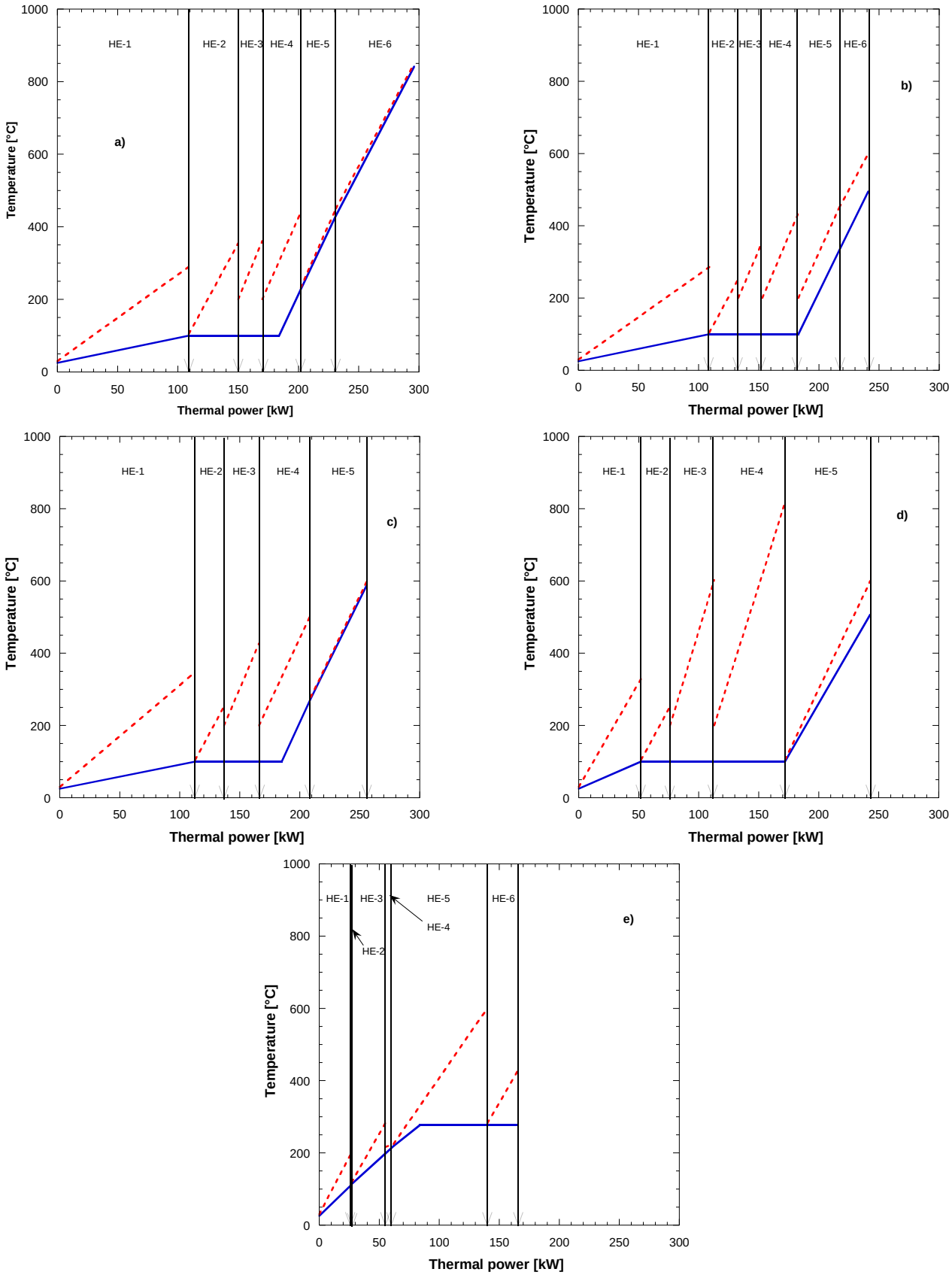

461 **Fig. 12.** Temperature-heat diagram of the heat recovery section (HRS); in red the hot gas stream, in blue the cold water side: a) case HR-1; b)
462 case HR-2; c) case HR-3; d) case PHR-1; e) case PHR-2.

Table 2. Thermal power at each HRS segment and external heat demand for the different analyzed configurations.

	Thermal power [kW]											
Case	**HE1**	**HE2**	**HE3**	**HE4**	**HE5**	**HE6**	**H_2O line total heat recovery**	**Sweep Air line heat recovery**	**External heat demand H_2O**	**External heat demand CO_2**	**External heat demand Sweep Air**	**Total external heat demand**
Reference Case	-	-	-	-	-	-	-	-	296.9	39.1	88.07	424.1
HR-1	109.2	41.0	19.9	31.4	29.3	65.0	295.7	87.5	1.3	39.1	0.57	41.0
HR-2	109.2	24.0	19.3	30.7	33.6	24.1	241.0	59.6	16.3	26.0	0.55	42.8
HR-3	112.9	24.0	29.5	42.2	47.2	-	255.7	59.6	1.6	26.0	0.55	28.2
PHR-1	51.8	23.9	37.6	59.1	70.2	-	242.6	59.6	14.4	26.0	0.55	40.9
PHR-2	26.6	0.3	27.7	7.2	78.2	24.6	164.5	30.8	87.1	6.4	0.55	94.1

The external heat demand is significantly reduced (by about 90%) with the adoption of the HRS (see **Table 2),** with a minimum value of 28.2 kW for case HR-3. In cases PHR-1 and PHR-2 the total external heat demand is higher with respect to the other configurations. In particular, it is equal to 40.9 kW for case PHR-1, while it is equal to 94.1 kW for case PHR-2. Moreover, it must be highlighted that, in all the heat recovery configurations, the external demand for the sweep air pre-heating is almost negligible, due to the internal heat recovery with the anodic outlet stream (see **Figs. 8-10**).

The electric-to-fuel conversion index and the compression electric power consumption normalized with respect to the SOEC power size are shown in **Fig. 13** for each analyzed configuration. The calculated η_{E2F} value is nearly the same (around 86%) for the Reference Case and for the configurations with only heat recovery (cases HR-1, HR-2 and HR-3), since the thermal power consumption is not included in this performance parameter. With the adoption of pressurization, η_{E2F} slightly decreases to a value of about 83% for case PHR-1 and to a value of about 80% for case PHR-2. These results can be mainly explained with the effect of the compression electric power consumption. As shown in **Fig. 13**, the normalized compression electric power consumption increases in the configurations with pressurization within the system: it is equal to 4.9% of the SOEC power size for case PHR-1 and it is equal to 7.8% for case PHR-2. The compression power depends on the mass flow rate of gas to be compressed: in the Reference Case and the cases HR-1, HR-2 and HR-3, where compression is the final step of the whole process after water separation, the produced gas mass flow rate is similar. On the other hand, in cases PHR-1 and PHR-1 the compression section occurs upstream the water separation, resulting in higher mass flow rates to be processed.

Values of the first-law efficiency and of the second-law efficiency are presented in **Fig. 14** for each analyzed configuration. The minimum value of η_I, equal to about 61%, is obtained for the Reference Case, where no heat recovery is implemented and the total external heat demand is considerably high (around 424 kW). On the contrary, the external heat demand to pre-heat the

water stream at the inlet of the co-electrolyzer is significantly lowered by the adoption of heat recovery within the system, allowing to reach higher values of η_I. In case HR-1, where the SOEC operating temperature is the same of the Reference Case (850 °C), the obtained η_I achieves value of about 83% with an increase of 22 percentage points with respect to the Reference Case. In the other two configurations (HR-2 and HR-3) with heat recovery but reduced SOEC operating temperature (600 °C), the η_I is not negatively affected by this reduction of temperature level, with similar η_I values. A slight increase is obtained in case HR-3, showing the highest obtained value, equal to 85%. In cases with system pressurization (PHR-1 and PHR-2), the η_I values are slightly reduced, due to the increased compression power consumption and a higher external heat demand. In particular, the calculated η_I value is equal to about 80% for case PHR-1, while it is equal to about 74% for case PHR-2.

The obtained values of η_{II} show a trend similar to the first-law efficiency, with a maximum value of about 79% for the case HR-3. The system configurations with pressurized methanation and SOEC still provide values of the second-law efficiency above 70%, with an increase of almost 10 percentage points in comparison with the system without heat recovery. As for the first law efficiency, these results are affected by the heat recovery section.

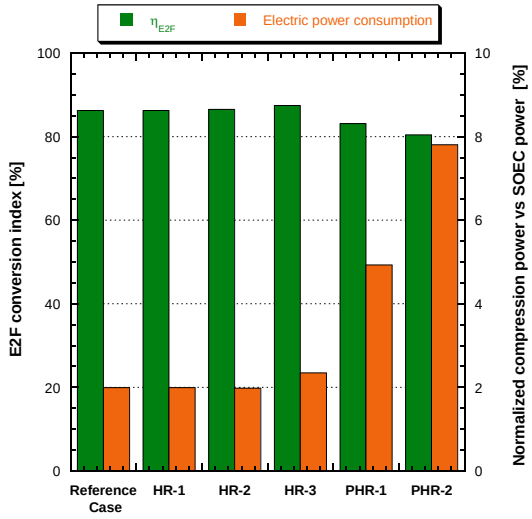

Fig. 13. η_{E2F} and normalized compression electric power consumption for the analyzed configurations.

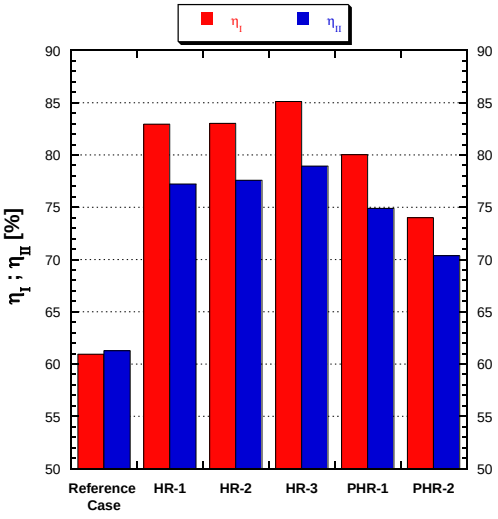

Fig. 14. η_I and η_{II} for the analyzed configurations.

In **Fig. 15** the composition of the produced SNG for the analyzed configurations is shown. In the first three cases, where the experimental reactor operating temperature is set at 450 °C (Reference Case, HR-1 and HR-2), the methane molar fraction in the produced SNG is almost constant, with a value of about 0.79. With the increase of the experimental reactor operating temperature up to a value of 600 °C (case HR-3), the reactor works outside the optimum operating range and the methanation reactions tend to shift towards the reactants. Indeed, in configuration HR-3 methane concentration falls down to a value of

about 0.64 and the hydrogen molar fraction increases up to a value of about 0.28. In order to introduce the produced SNG into the NG distribution network, the hydrogen content is considered a negative aspect, due to the restrictions on the maximum hydrogen molar fraction. On the other hand, from the point of view of the SNG chemical power, hydrogen allows to achieve higher values of the HHV index. This effect, led by the change of the experimental reactor operating temperature, is balanced by the pressurization of the methanation section. As it can be seen in the figure, in cases PHR-1 and PHR-2, where experimental reactor operating temperature is set to a value of 600 °C, the methane content in the produced SNG increases. In particular, in configuration PHR-1, where only the TREMP^{TM} methanation section is pressurized, the methane molar fraction reaches the value of about 0.96, while in configuration PHR-2, where the whole system is pressurized, the produced SNG is nearly a pure methane stream.

The composition of the produced SNG affects the quality indexes of the fuel stream, as it can be seen in **Fig. 16,** where the HHV, the WI and the SG of the produced SNG are presented. In order to introduce the produced SNG into the NG distribution network some technical specifications must be checked. In this study, specifications required by Italian legislation [47] have been considered. These prescriptions provide ranges of acceptability mainly for the HHV, for the SG and for the WI. In more detail, the ranges of acceptability are:

- 34950 kJ/Sm^3 ≤ HHV ≤ 45280 kJ/Sm^3;
- 47310 kJ/Sm^3 ≤ WI ≤ 52330 kJ/Sm^3;
- 0.5548 ≤ SG ≤ 0.8000.

As it can be seen in the figure, the cases with a low methane concentration (Reference Case, HR-1, HR-2 and HR-3) show a produced SNG with properties outside the ranges of acceptability. Regarding the HHV and the WI, only cases PHR-1 and PHR-2 are acceptable: case PHR-1 presents a produced SNG with HHV value 36392 kJ/Sm^3 and a WI of 49086 kJ/Sm^3, while the SNG produced by PHR-2 shows HHV value of 37364 kJ/Sm^3 and a WI of 50079 kJ/Sm^3. On the other hand, considering the SG assumed values, only configuration PHR-2 is acceptable with a value of 0.5567. The configuration PHR-1 shows a produced SNG with a SG value slightly lower than the lower SG limit and equal to 0.5497. In this situation the produced SNG can be correct with a diluent (*e.g.* nitrogen), in order to increase the density. However, the dilution of the produced SNG causes the lowering of the HHV and of the WI with the potential of being outside the acceptability ranges of these two parameters.

In order to give some directions for real applications, the obtained results can be summarized as it follows:

i. the thermal integration between co-SOEC and methanation reactor – considering an intermediate operating temperature level with respect to the typical ones of the two separate components – represents a feasible solution, allowing to achieve good performance parameters. This result can lead to the possibility of physically integrate co-

electrolyzer and methanation reactor for further innovative P2G technology development and system architecture simplification;

ii. in case of SNG produced for the introduction into a NG network, a configuration with thermal integration, heat recovery and pressurization can be seen as the best solution, allowing to achieve the higher values of methane content, HHV, Wobbe index and SG with still acceptable values of energy conversion and thermodynamic efficiencies;

iii. in case of no constraint on the produced SNG quality (*e.g.*, for applications different from the NG network introduction), the configuration which enables to minimize the primary energy consumption (*i.e.*, maximizing the efficiency indicators) is the one with thermal integration and heat recovery. Furthermore, in this case, all the system components work at ambient pressure, with a consequent simplification of the P2G system operation.

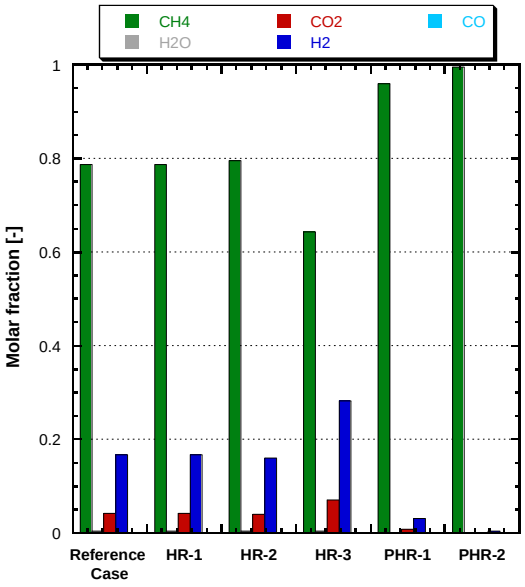

Fig. 15. Composition of the produced SNG for the analyzed configurations.

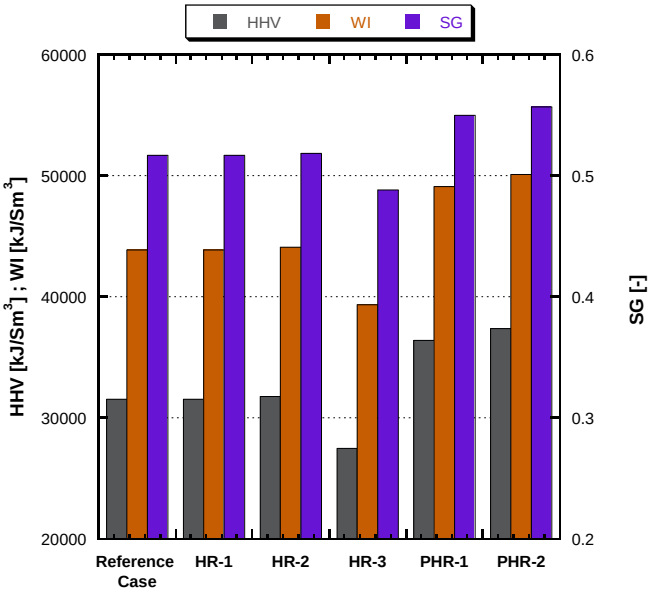

Fig. 16. HHV, WI and SG of the produced SNG for the analyzed configurations.

6. Conclusions

In this paper an innovative Power-to-Gas storage system based on a high temperature co-electrolyzer (operating in the range 600-850 °C) and a methanation section based on structured catalyst (operating at 450-600 °C) has been investigated, considering various layout configurations. The model developed in ASPEN environment is able to reproduce the thermodynamic behavior of the Power-to-Gas system. The thermal balance of plant has been numerically simulated including all the main thermal flows. The performed study provided the following main findings:

- the possibility to thermally integrate the co-electrolyzer and the high temperature methanation section has been demonstrated;
- internal heat recovery is mandatory, in order to achieve high values of first-law efficiency and second-law efficiency. The peak calculated value of first-law efficiency is 85%, while the peak value of second-law efficiency is 79%.
- Pressurization of the methanation section and of the co-electrolysis section produces a reduction in the efficiency values, but it allows to obtain a final composition of the synthetic natural gas with methane fraction close to 100%.
- The quality of the produced synthetic fuel in terms of Wobbe Index, HHV and specific gravity is reduced, if pressurization is not implemented but it could be improved if additional conventional methanation sections or membrane would be applied at the end of the process.

Acknowledgments

This research was supported by Ricerca di Sistema (RdS-CNR PAR 2015-17), Italian ministerial founding for researches on the electric systems.

Nomenclature

ex	Specific mass exergy [kJ/kg]
Ex	Exergy [kJ]
GHSV	Gas hourly space velocity [h^{-1}]
h	Specific mass enthalpy [kJ/kg]
HHV	Higher heating value [kJ/kg] or [kJ/Sm^3]
LHV	Lower heating value [kJ/kg]
$\dot{m}$	Mass flow rate [kg/s]
M_m	Molecular mass [kg/kmol]
$\dot{n}$	Molar flow rate [kmol/s]
P	Power [kW]
p	Pressure [bar]
Q	Thermal power [kW]
R_0	Universal gas constant [kJ/kmolK]
s	Specific mass entropy [kJ/kgK]

SG	Specific gravity [-]
T	Temperature [°C]
WI	Wobbe index [kJ/Sm^3]
y_i	Molar fraction of the i-th component [-]

Greek symbols

Δ	Difference
η	Efficiency
ρ	Density [kg/m^3]

Subscripts and Superscripts

Air	for air stream
C1	Compressor C1
C2	Compressor C2
Chem	Chemical
CO2	for CO_2 stream
e	Electric
el	Electrical
f	Flux
in	Inlet
m	Molecular
Mix	Mixing
mol	Molar
out	Outlet
Ph	Physical

Acronyms

C	Compression
CCS	Carbon capture and storage
CR	Conversion rate
E2F	Electric-to-fuel

GDC	Gadolinium-Doped-Ceria
GHG	Greenhouse gas
HE	Heat recovery section heat exchanging segment
HR	Heat recovery
HRS	Heat recovery section
HT	High temperature
HTE	High temperature electrolyzer
HTM	High temperature methanation
HX	Heat exchanger
IC	Inter-cooler
Liq	Liquid
LT	Low temperature
LTE	Low temperature electrolyzer
LTM	Low temperature methanation
NG	Natural gas
NP-RES	Non-programmable renewable energy sources
P	Pump
PEM	Proton exchange membrane
PHR	Pressurized heat recovery
P2G	Power-to-gas
R	Reactor
RES	Renewable energy sources
SCS	Solution Combustion Synthesis
Sep	Separation
SOEC	Solid oxide electrolyte cell
SNG	Synthetic natural gas
TREMP	Topsøe Recycle Energy-efficient Methanation Process
I	First law of thermodynamics
II	Second law of thermodynamics

References

1. "Statistics: Key electricity trends 2016", https://www.iea.org , 2017.
2. Eltawil, M. A., & Zhao, Z. (2010). Grid-connected photovoltaic power systems: Technical and potential problems—A review. *Renewable and Sustainable Energy Reviews*, *14*(1), 112-129.
3. Chalmers, S. M., Hitt, M. M., Underhill, J. T., Anderson, P. M., Vogt, P. L., & Ingersoll, R. (1985). The effect of photovoltaic power generation on utility operation. *IEEE Transactions on Power Apparatus and Systems*, (3), 524-530.
4. Jewell, W. T., Ramakumar, R., & Hill, S. R. (1988). A study of dispersed photovoltaic generation on the PSO system. *IEEE Transactions on Energy Conversion*, *3*(3), 473-478.
5. Luo, X., Wang, J., Dooner, M., Clarke, J. (2015). Overview of current development in electrical energy storage technologies and the application potential in power system operation. *Applied Energy*, *137*, 511–536
6. Arani, A. K., Karami, H., Gharehpetian, G. B., & Hejazi, M. S. A. (2017). Review of Flywheel Energy Storage Systems structures and applications in power systems and microgrids. *Renewable and Sustainable Energy Reviews*, *69*, 9-18.
7. Akinyele, D. O., & Rayudu, R. K. (2014). Review of energy storage technologies for sustainable power networks. *Sustainable Energy Technologies and Assessments*, *8*, 74-91.
8. Aneke, M., & Wang, M. (2016). Energy storage technologies and real life applications–A state of the art review. *Applied Energy*, *179*, 350-377.
9. Castillo, A., & Gayme, D. F. (2014). Grid-scale energy storage applications in renewable energy integration: A survey. *Energy Conversion and Management*, *87*, 885-894.
10. Blanco, H., & Faaij, A. (2018). A review at the role of storage in energy systems with a focus on Power to Gas and long-term storage. *Renewable and Sustainable Energy Reviews*, *81*, 1049-1086.
11. Götz, M., Lefebvre, J., Mörs, F., Koch, A. M., Graf, F., Bajohr, S., ... & Kolb, T. (2016). Renewable Power-to-Gas: A technological and economic review. Renewable energy, 85, 1371-1390.
12. Schiebahn, S., Grube, T., Robinius, M., Tietze, V., Kumar, B., & Stolten, D. (2015). Power to gas: Technological overview, systems analysis and economic assessment for a case study in Germany. *International Journal of Hydrogen Energy*, *40*(12), 4285-4294.
13. Rönsch, S., Schneider, J., Matthischke, S., Schlüter, M., Götz, M., Lefebvre, J., ... & Bajohr, S. (2016). Review on methanation–From fundamentals to current projects. Fuel, 166, 276-296.
14. Wei, W., & Jinlong, G. (2011). Methanation of carbon dioxide: an overview. *Frontiers of Chemical Science and Engineering*, *5*(1), 2-10.

15. MacDowell, N., Florin, N., Buchard, A., Hallett, J., Galindo, A., Jackson, G., ... & Fennell, P. (2010). An overview of CO_2 capture technologies. *Energy & Environmental Science*, *3*(11), 1645-1669.
16. Eveloy, V., Gebreegziabher, T. A Review of Projected Power-to-Gas Deployment Scenarios, Energies 2018, 11(7), 1824; doi:10.3390/en11071824
17. Buttler, A., & Spliethoff, H. (2018). Current status of water electrolysis for energy storage, grid balancing and sector coupling via power-to-gas and power-to-liquids: A review. *Renewable and Sustainable Energy Reviews*, *82*, 2440-2454.
18. Schmidt, O., Gambhir, A., Staffell, I., Hawkes, A., Nelson, J., & Few, S. (2017). Future cost and performance of water electrolysis: An expert elicitation study. *International journal of hydrogen energy*, *42*(52), 30470-30492.
19. Laguna-Bercero, M. A. (2012). Recent advances in high temperature electrolysis using solid oxide fuel cells: A review. *Journal of Power sources*, *203*, 4-16.
20. HELMET EU project; http://www.helmeth.eu/
21. Sapountzi, F. M., Gracia, J. M., Fredriksson, H. O., & Niemantsverdriet, J. H. (2017). Electrocatalysts for the generation of hydrogen, oxygen and synthesis gas. *Progress in Energy and Combustion Science*, *58*, 1-35.
22. Ivy, J. (2004). *Summary of electrolytic hydrogen production: milestone completion report* (No. NREL/MP-560-36734). National Renewable Energy Lab., Golden, CO (US).
23. Wang, L., Pérez-Fortes, M., Madi, H., Diethelm, S., & Maréchal, F. (2018). Optimal design of solid-oxide electrolyzer based power-to-methane systems: A comprehensive comparison between steam electrolysis and co-electrolysis. *Applied Energy*, *211*, 1060-1079.
24. Bailera, M., Lisbona, P., Romeo, L. M., & Espatolero, S. (2017). Power to Gas projects review: Lab, pilot and demo plants for storing renewable energy and CO_2. *Renewable and Sustainable Energy Reviews*, *69*, 292-312.
25. Giglio, E., Lanzini, A., Santarelli, M., & Leone, P. (2015). Synthetic natural gas via integrated high-temperature electrolysis and methanation: Part I—Energy performance. *Journal of Energy Storage*, *1*, 22-37.
26. Vita, A., Italiano, C., Pino, L., Frontera, P., Ferraro, M., & Antonucci, V. (2018). Activity and stability of powder and monolith-coated Ni/GDC catalysts for CO_2 methanation. *Applied Catalysis B: Environmental*.
27. Ancona, M.A., Antonioni, G., Branchini, L., De Pascale, A., Melino, F., Orlandini, V., Antonucci, V., Ferraro, M. (2016) Renewable Energy Storage System Based on a Power-to-Gas Conversion Process. *Energy Procedia*, 101, 854-861.
28. Ancona, M.A., Antonucci, V., Branchini, L., Catena, F., De Pascale, A., Di Blasi, A., Ferraro, M., Italiano, C., Melino, F., Vita, A. (2018). Performance of a Power-to-Gas Energy Storage System based on Integrated High Temperature co-Electrolysis and Methanation. *Proceedings of 13th Conference on Sustainable Development of Energy, Water and Environment Systems*, September 30 – October 4 (2018), Palermo, Italy.

29. Lo Faro, M., Zignani, S.C., Trocino, S., Antonucci, V., Aricò, A.S. (2019). New insights on the co-electrolysis of CO_2 and H_2O through a solid oxide electrolyser operating at intermediate temperatures. *Electrochimica Acta*, *296*, 458-464.
30. Topsoe, H. (2009). From solid fuels to substitute natural gas (SNG) using TREMP. *Technocal Report, Halder Topsoe*.
31. Zheng, Y., Wang, J., Yu, B., Zhang, W., Chen, J., Qiao, J., & Zhang, J. (2017). A review of high temperature co-electrolysis of H_2O and CO_2 to produce sustainable fuels using solid oxide electrolysis cells (SOECs): advanced materials and technology. *Chemical Society Reviews*, *46*(5), 1427-1463.
32. Aspen Hysys™; https://www.aspentech.com/
33. Redissi, Y., & Bouallou, C. (2013). Valorization of carbon dioxide by co-electrolysis of CO_2/H_2O at high temperature for syngas production. *Energy Procedia*, *37*, 6667-6678.
34. Sun, X., Chen, M., Jensen, S. H., Ebbesen, S. D., Graves, C., & Mogensen, M. (2012). Thermodynamic analysis of synthetic hydrocarbon fuel production in pressurized solid oxide electrolysis cells. *International journal of hydrogen energy*, *37*(22), 17101-17110.
35. Mehran, M. T., Yu, S. B., Lee, D. Y., Hong, J. E., Lee, S. B., Park, S. J., ... & Lim, T. H. (2018). Production of syngas from H_2O/CO_2 by high-pressure coelectrolysis in tubular solid oxide cells. *Applied Energy*, *212*, 759-770.
36. Samavati, M., Santarelli, M., Martin, A., & Nemanova, V. (2017). Thermodynamic and economy analysis of solid oxide electrolyser system for syngas production. *Energy*, *122*, 37-49.
37. Stoots, C. M., O'Brien, J.E., Herring, J. S., Hartvigsen, J. J. (2009). Syngas production via high-temperature coelectrolysis of steam and carbon dioxide. *Journal of fuel cell science and technology*, *6*(1), 011014, doi:10.1115/1.2971061.
38. Stempien, J. P., Ding, O. L., Sun, Q., & Chan, S. H. (2012). Energy and exergy analysis of Solid Oxide Electrolyser Cell (SOEC) working as a CO_2 mitigation device. *International Journal of Hydrogen Energy*, *37*(19), 14518-14527.
39. Ebbesen, S. D., Høgh, J., Nielsen, K. A., Nielsen, J. U., & Mogensen, M. (2011). Durable SOC stacks for production of hydrogen and synthesis gas by high temperature electrolysis. *International Journal of Hydrogen Energy*, *36*(13), 7363-7373.
40. Jensen, J. H., Poulsen, J. M., & Andersen, N. U. (2011). From coal to clean energy. *Nitrogen+ syngas*, *310*, 34-38.
41. Kim, S. W., Kim, H., Yoon, K. J., Lee, J. H., Kim, B. K., Choi, W., ... & Hong, J. (2015). Reactions and mass transport in high temperature co-electrolysis of steam/CO2 mixtures for syngas production. *Journal of Power Sources*, *280*, 630-639.
42. Graves, C., Ebbesen, S. D., & Mogensen, M. (2011). Co-electrolysis of CO2 and H2O in solid oxide cells: performance and durability. *Solid State Ionics*, *192*(1), 398-403.
43. Snam Rete Gas – Italian National Natural Gas Utility. http://www.snam.it/it/index.html
44. Koytsoumpa, E. I., & Karellas, S. (2018). Equilibrium and kinetic aspects for catalytic methanation focusing on CO_2 derived Substitute Natural Gas (SNG). *Renewable and Sustainable Energy Reviews*, *94*, 536-550.

45. Rosen, M. A., & Dincer, I. (2001). Exergy as the confluence of energy, environment and sustainable development. *Exergy, an International journal*, *1*(1), 3-13.

46. Kaushik, S. C., Reddy, V. S., & Tyagi, S. K. (2011). Energy and exergy analyses of thermal power plants: A review. *Renewable and Sustainable energy reviews*, *15*(4), 1857-1872.

47. Ministero dello Sviluppo Economico, Approvazione della regola tecnica sulle caratteristiche chimico-fisiche e sulla presenza di altri componenti nel gas combustibile da convogliare,(2007). In Italian, available at: http://www.gazzettaufficiale.it/eli/gu/2007/03/19/65/sg/pdf

Appendix A

Reference Case

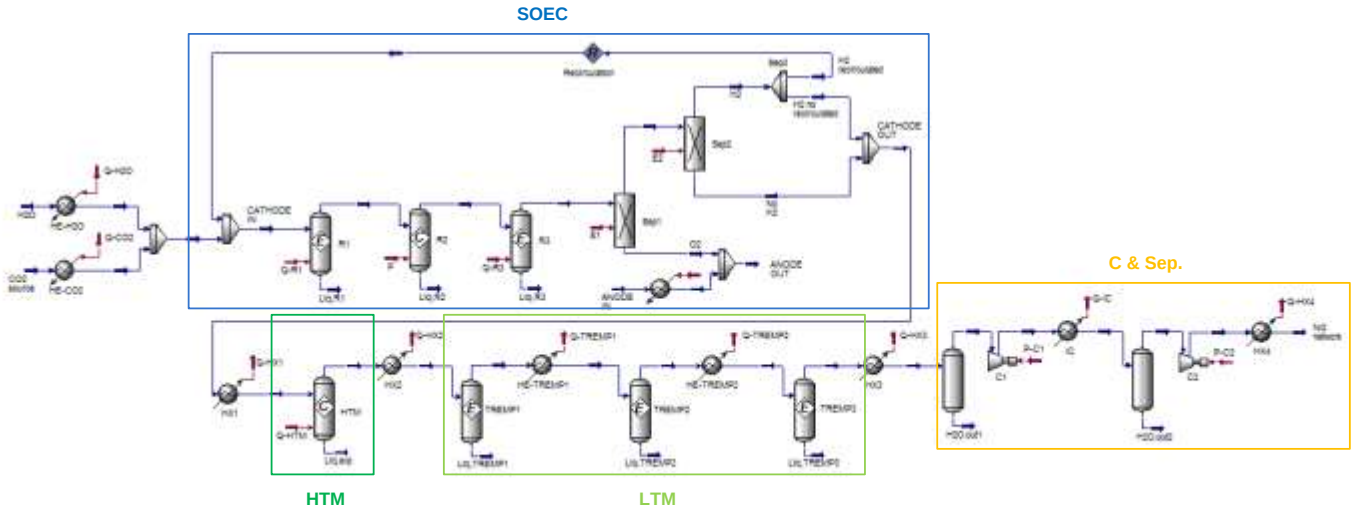

Fig. A1. Reference Case model on ASPEN Hysys™.

Cases HE-1 and HE-2

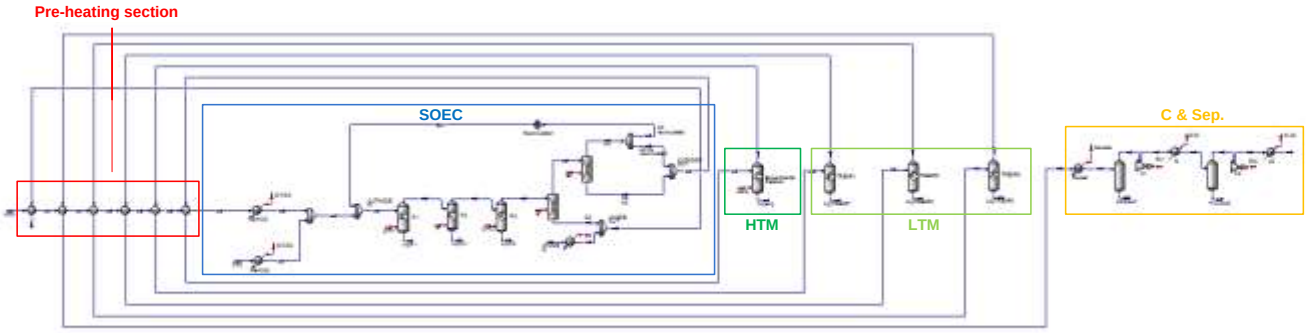

Fig. A2. Cases HE-1 and HE-2 model on ASPEN Hysys™.

Case HE-3

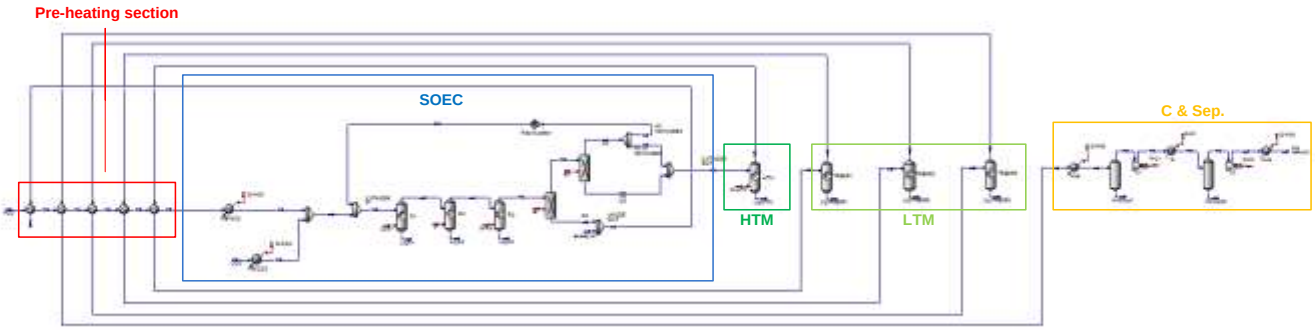

Fig. A3. Case HE-3 model on ASPEN Hysys™.

Case PHR-1

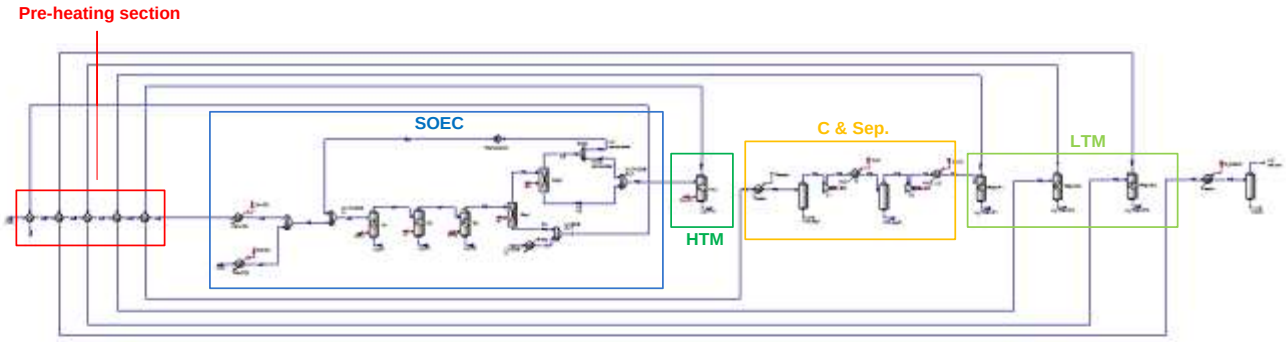

Fig. A4. Case PHR-1 model on ASPEN Hysys™.

Case PHR-2

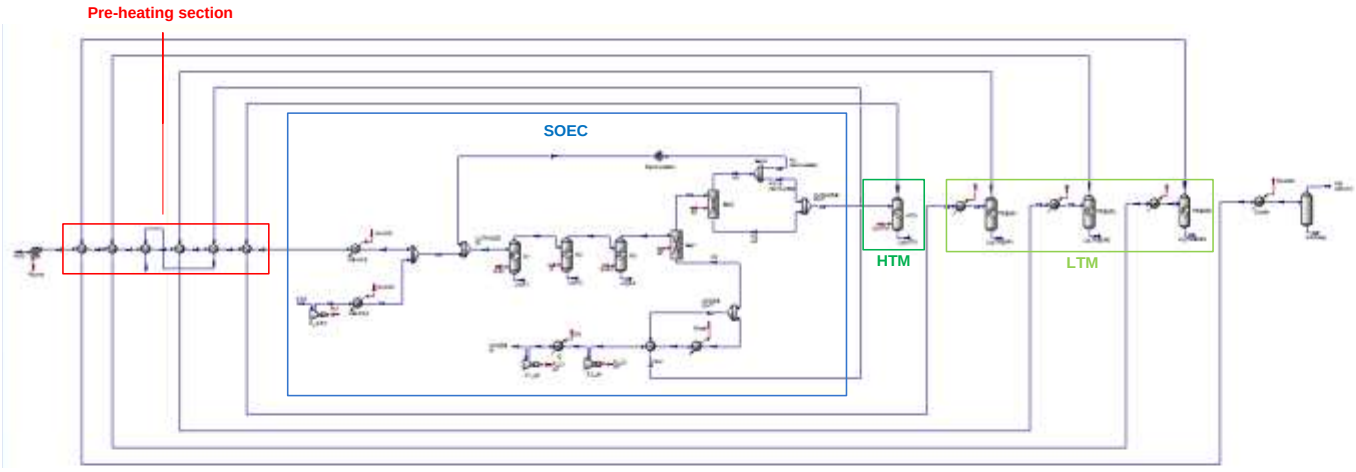

Fig. A5. Case PHR-2 model on ASPEN Hysys™.